SIAM J. SCI. COMPUT.
Vol. 28, No. 6, pp. 2001–2022


# A FULLY MASS AND VOLUME CONSERVING IMPLEMENTATION OF A CHARACTERISTIC METHOD FOR TRANSPORT PROBLEMS*

TODD ARBOGAST† AND CHIEH-SEN HUANG‡

**Abstract.** The characteristics-mixed method considers the transport not of a single point or fluid particle, but rather the mass in an entire region of fluid. This mass is transported along the characteristic curves of the hyperbolic part of the transport equation, and the scheme thereby produces very little numerical dispersion, conserves mass locally, and can use long time steps. However, since the shape of a characteristic trace-back region must be approximated in numerical implementation, its volume may be incorrect, resulting in inaccurate concentration densities and, further, inaccurate reaction dynamics. We present a simple modification to the characteristics-mixed method that conserves both mass and volume of the transported fluid regions. Our algorithm also handles boundary conditions through a space-time change of variables in the trace-back routines, which allows the boundary to be treated as if it were interior to the domain. Nearly point sources, such as wells, present special difficulties, since characteristic trace-back curves converge in their vicinity. We also present techniques that allow one to conservatively implement wells. The techniques are illustrated in five numerical examples.

**Key words.** advection-diffusion, characteristics-mixed method, ELLAM, mixed finite element, local conservation, porous media

**AMS subject classifications.** 65M25, 76M25, 76S05

**DOI.** 10.1137/040621077

## 1. Introduction.

We consider in this paper the problem of tracer transport in a flow field, as might arise in a porous medium or a shallow water or atmospheric system. We concentrate on the problem as it arises in porous media simulation, though many of the ideas carry over to other contexts.

Let $\Omega \subset \mathbb{R}^2$ be our bounded domain, and consider an incompressible bulk fluid of velocity $\mathbf{u}(\mathbf{x}, t)$ satisfying the incompressibility condition

$$\nabla \cdot \mathbf{u} = q, \quad \Omega \times J, \tag{1.1}$$

where $q(\mathbf{x}, t)$ is a given external source or sink function, assumed smooth enough for our purposes, and $J = (0, \infty)$ is the time interval. Our interest lies in the transport of some dilute tracer or other solute species of concentration $c(\mathbf{x}, t)$ within the bulk fluid. We assume that it does not change the overall velocity $\mathbf{u}$. The concentration will generally satisfy an advection-diffusion equation of the form

$$(R\phi c)_t + \nabla \cdot (c\mathbf{u} - D\nabla c) = c_I q_+ + c q_- \equiv q_c(c), \quad \Omega \times J, \tag{1.2}$$

where $R(\mathbf{x})$ is the retardation factor, $\phi(\mathbf{x})$ is the storage factor of the medium called porosity, subscript $t$ is time partial differentiation, $D(\mathbf{x}, t)$ is the diffusion/dispersion

*Received by the editors December 17, 2004; accepted for publication (in revised form) May 15, 2006; published electronically December 5, 2006.
http://www.siam.org/journals/sisc/28-6/62107.html

†Department of Mathematics, The University of Texas at Austin, 1 University Station C1200, Austin, TX 78712, and Institute for Computational Engineering and Sciences, The University of Texas at Austin, 1 University Station C0200, Austin, TX 78712 (arbogast@ices.utexas.edu). This author was supported in part by U.S. National Science Foundation grant DMS-0417431.

‡Corresponding author. Department of Applied Mathematics and National Center for Theoretical Sciences, National Sun Yat-sen University, Kaohsiung 804, Taiwan, R.O.C. (huangcs@math.nsysu.edu.tw).

coefficient (that may also depend on $\mathbf{u}$), $q_+(\mathbf{x},t) \geq 0$ is $q$ when $q > 0$ and 0 otherwise, $q_-(\mathbf{x},t) = q - q_+ \leq 0$, and $c_I(\mathbf{x},t)$ is the given concentration of injected fluid.

To apply characteristic methods to (1.2), one generally uses an operator splitting technique to isolate the hyperbolic and parabolic parts of the equation. That is, over a time step, one approximates the hyperbolic part of the operator,

$$(R\phi c)_t + \nabla \cdot (c\mathbf{u}) = q_c(c), \quad \Omega \times J, \tag{1.3}$$

and the parabolic part,

$$(R\phi c)_t - \nabla \cdot (D\nabla c) = 0, \quad \Omega \times J, \tag{1.4}$$

in some order. We discuss neither the operator splitting nor the approximation of the parabolic part in this paper.

The hyperbolic part of (1.3) is the most delicate to approximate well. It models pure transport of the fluid particles, while the rest of the operator, $-\nabla \cdot (D\nabla c)$, is diffusive. In the absence of shocks and diffusion, fluid particles simply travel along the characteristics of (1.3) (see (2.2) below). The fluid must obey two principles: *tracer mass conservation* and incompressibility, or, loosely speaking, *volume conservation* (i.e., mass conservation of the incompressible bulk fluid). The first principle is well known; we make the second precise in the next section, but basically, for an incompressible fluid, the volume occupied by a given amount of mass is fixed.

Numerical methods based on fixed grids, such as Godunov's method [15], are locally mass conservative by design. They are also automatically volume conserving, since the volumes of the fixed grid elements do not change in time.

Moving mesh and characteristic methods, however, do not automatically conserve volume. Characteristic methods became viable when Douglas and Russell described their *modified method of characteristics* in 1982 [12]. In their method, one approximates the characteristic derivative by a finite difference in the characteristic direction; that is,

$$c_\tau(\mathbf{x},t) \equiv c_t(\mathbf{x},t) + \frac{\mathbf{u}(\mathbf{x},t)}{R\phi} \cdot \nabla c(\mathbf{x},t) \approx \frac{c(\mathbf{x},t+\Delta t) - c(\hat{\mathbf{x}},t)}{\Delta t} \ ,$$

where $\mathbf{x}$ is a grid point, $\Delta t > 0$, and $\hat{\mathbf{x}}$ is defined by tracing the point $(\mathbf{x}, t+\Delta t)$ backwards in time along the characteristics to $(\hat{\mathbf{x}}, t)$ (see section 2). This results in the approximation

$$R\phi \frac{c(\mathbf{x},t+\Delta t) - c(\hat{\mathbf{x}},t)}{\Delta t} = (c_I - c)q_+$$

of (1.3). Because the method is based on points, it violates *both* local mass and volume constraints. A subsequent modification produced a global mass balance [10], but not a local mass balance.

Various ELLAM [6] schemes have been developed based on the local mass constraint, including the characteristics-mixed method [2, 3] and its two-phase variant [11]. The basic idea is to trace back along the characteristics each entire grid element $E$ to $\hat{E}$. In this way, all mass can be accounted for locally; that is, all the mass in $\hat{E}$ is numerically transported forward into $E$. In the absence of sources, sinks, and external boundaries, the volumes of $E$ and $\hat{E}$ agree. However, to trace $\hat{E}$ back in time requires tracing each boundary point back, which can only be done in one space dimension (unless perhaps the velocity is particularly simple). So, in practice, one

must approximate $\hat{E}$ by some simpler shape $\tilde{E}$ by, say, tracing back only the vertices of the element. Almost assuredly the volumes of $\tilde{E}$ and $\hat{E}$ will disagree, violating the volume conservation principle.

Although mass is conserved locally, incorrect local volumes lead to incorrect concentrations, which measure mass per volume. That is, the density is incorrectly approximated and can lead to overshoot or undershoot and seriously degrade the quality of the solution over time, especially when reaction dynamics, based on densities, are also considered.

We present in this paper a simple and relatively computationally efficient method for adjusting the trace-back regions $\hat{E}$ to $\tilde{E}$. The difficulty, of course, is that the set of $\tilde{E}$ must tessellate the region (i.e., they must have no overlaps or gaps). For simplicity of exposition, we consider in this paper only a two-dimensional (2-D) domain and a rectangular grid of elements. In principle, our ideas should generalize to other grids and even to three dimensions, but we expect the difficulty of implementation to be considerable, and so we have no numerical experience to report for these cases at this time.

A more computationally expensive method was proposed by Chilakapati [7, 8]. He proposed a procedure that modifies the way in which the Darcy velocity itself is computed and then applies this to the advection equation.

An outline of this paper follows. We define the characteristics in the next section, and point out that our techniques cannot handle multiple characteristics as might arise in multiphase flow. In section 3, we then carefully derive the local mass and volume constraints. Since sources and sinks in porous media simulation arise from wells, which are very small, the source terms must be approximated carefully. Similar to sources are inflow boundaries, where $\mathbf{u}\cdot\nu < 0$ and points track out of the domain as time reverses. When the flow is not too strong, we have simple techniques for handling injection wells and inflow boundaries, as described in sections 4 and 5. Our trace-back point volume adjustment algorithm is described in section 6. For stronger flows, it is more effective to use a trace-forwarding technique to treat injection wells (and perhaps inflow boundaries), as presented in section 7. The final section is devoted to five numerical examples illustrating the need for volume adjustment and showing the efficacy of the proposed scheme.

**2. Characteristic trace-back.** In the absence of diffusion and dispersion (i.e., $D = 0$), fluid particles governed by (1.3) travel along paths called characteristics. In multiphase flow problems, there are multiple characteristics, as each phase flows at its own speed. We allow here only the relatively simple situation of linear adsorption, with a single fluid phase and a single incompressible solid phase. Assuming adsorption of the tracer but not the bulk fluid, the bulk and tracer fluid particles travel at different speeds. This can be seen more easily if the medium is considered as being compressible, i.e., $\phi$ depends also on time. Then (1.1) should be written as

$$\phi_t + \nabla \cdot \mathbf{u} = q, \quad \Omega \times J,$$

and we see that bulk fluid particles flow with velocity $\mathbf{u}/\phi$. However, tracer particles flow with velocity $\mathbf{u}/R\phi$, which is not the same if $R \neq 1$. Multiple characteristics cause difficulties, so we have assumed incompressibility of the medium ($\phi$ and $R$ depend only on $\mathbf{x}$). Then (1.1) is equivalent to

$$(R\phi)_t + \nabla \cdot \mathbf{u} = q, \quad \Omega \times J, \tag{2.1}$$

with characteristic speed $\mathbf{u}/R\phi$. We remark that we could have instead assumed that $R = 1$ and allowed $\phi$ to depend on $t$. Our technique extends to this case.

We consider only flow during a time step, so let $\Delta t > 0$ be given and $t^n = n\Delta t$ for $n = 0, 1, \ldots$. As is usual, for a generic function $\varphi$, we denote $\varphi(t^n)$ by $\varphi^n$. The time interval of interest is $[t^n, t^{n+1}]$. The characteristic trace-back of the point $\mathbf{x} \in \Omega$ is denoted $\hat{\mathbf{x}} = \hat{\mathbf{x}}(\mathbf{x}; t)$, and it satisfies the (time backward) ordinary differential equation

$$\frac{d\hat{\mathbf{x}}}{dt} = \frac{\mathbf{u}(\hat{\mathbf{x}}, t)}{R(\hat{\mathbf{x}})\phi(\hat{\mathbf{x}})}, \quad t^n \le t < t^{n+1}, \tag{2.2}$$

$$\hat{\mathbf{x}}(t^{n+1}) = \mathbf{x}, \tag{2.3}$$

unless the particle traces to the boundary of the domain or is created at an external source. In either of these two exceptional cases, the particle arises from the outside world and must be treated accordingly.

**3. The local mass and volume constraints.** Let $\mathcal{T}$ be a finite partition of $\Omega$ into closed elements with disjoint interiors; that is, $\bar{\Omega} = \bigcup_{E\in\mathcal{T}} E$ and $\overset{\circ}{E}_i \cap \overset{\circ}{E}_j = \emptyset$ for all $i \ne j$. Often in our discussion $\mathcal{T}$ can be an arbitrary partition of $\Omega$; however, sometimes we need more structure, so we tacitly assume that both $\Omega$ and the partition $\mathcal{T}$ are rectangular, with $\mathcal{T}$ having $M\times N$ elements. We use the usual Cartesian labeling of the grid points $\mathbf{x}_{i,j} = (x_i, y_j)$, where $i = 1, 2, \ldots, M+1$ and $j = 1, 2, \ldots, N+1$, and $x_i < x_{i+1}$ and $y_j < y_{j+1}$. Then rectangular element $E_{i,j} \in \mathcal{T}$ has vertices $\{\mathbf{x}_{i,j}, \mathbf{x}_{i+1,j}, \mathbf{x}_{i,j+1}, \mathbf{x}_{i+1,j+1}\}$. We also denote the midpoints of the element edges as $\mathbf{x}_{i+1/2,j} = (x_{i+1/2}, y_j)$ and $\mathbf{x}_{i,j+1/2} = (x_i, y_{j+1/2})$, where $x_{i+1/2} = (x_i + x_{i+1})/2$ and $y_{j+1/2} = (y_j + y_{j+1})/2$.

The key idea used to obtain mass conserving characteristic methods is to trace regions rather than points, an idea due to Arbogast and Wheeler [2, 3]. The particles in $E \in \mathcal{T}$ trace back to a region we call $\hat{E}$, defined by

$$\hat{E} = \{\hat{\mathbf{x}} \in \Omega : \hat{\mathbf{x}} = \hat{\mathbf{x}}(\mathbf{x}; t^n) \text{ for some } \mathbf{x} \in E\}.$$

In space and time, we actually trace a region $\mathcal{E} = \mathcal{E}(E)$ given by

$$\mathcal{E} = \{(\hat{\mathbf{x}}, t) \in \Omega \times [t^n, t^{n+1}] : \hat{\mathbf{x}} = \hat{\mathbf{x}}(\mathbf{x}; t) \text{ for some } \mathbf{x} \in E\}.$$

We decompose $\partial\mathcal{E}$ into three regions, viewing time as going "up." Then the "top" is $E$, where $t = t^{n+1}$; the "bottom" is $\hat{E}$, where $t = t^n$; and the "sides" we call $\mathcal{S}$. The sides come in two flavors. If particles trace back to the boundary of the domain, we have $\mathcal{S}_B = \partial\mathcal{E} \cap \partial\Omega \times (t^n, t^{n+1})$. Otherwise, we have the more usual interior side $\mathcal{S}_I = \partial\mathcal{E} \cap \Omega \times (t^n, t^{n+1})$. That is, we have the disjoint union

$$\partial\mathcal{E} = E \cup \hat{E} \cup \mathcal{S} = E \cup \hat{E} \cup \mathcal{S}_I \cup \mathcal{S}_B.$$

Local mass conservation of the tracer can be obtained over $E \in \mathcal{T}$ by integrating (1.3) in space-time over $\mathcal{E}$ and using the divergence theorem [3]. First, if $d\sigma$ is the space-time boundary differential on $\partial\mathcal{E}$, we compute

$$\begin{aligned}
\iint_{\mathcal{E}} q_c \, dx\, dt &= \iint_{\mathcal{E}} \nabla_{x,t} \cdot \begin{pmatrix} c\mathbf{u} \\ R\phi c \end{pmatrix} dx\, dt \\
&= \iint_{\partial\mathcal{E}} c \begin{pmatrix} \mathbf{u} \\ R\phi \end{pmatrix} \cdot \nu_{x,t} \, d\sigma \\
&= \int_E R\phi c^{n+1} \, dx - \int_{\hat{E}} R\phi c^n \, dx + \int_{\mathcal{S}} c \begin{pmatrix} \mathbf{u} \\ R\phi \end{pmatrix} \cdot \nu_{x,t} \, d\sigma,
\end{aligned}$$

since on the top and bottom of the domain $\nu_{x,t} = (0, \pm 1)$. The last term is integration on the space-time sides $\mathcal{S}$ of $\mathcal{E}$. Because the region $\mathcal{E}$ is defined by following characteristics, $\binom{\mathbf{u}}{R\phi}$ is orthogonal to $\nu_{x,t}$ on $\mathcal{S}_I$, that is, on $\mathcal{S}$ unless we have traced to the boundary of the domain. Thus the last term is

$$\int_{\mathcal{S}} c \binom{\mathbf{u}}{R\phi} \cdot \nu_{x,t} \, d\sigma = \int_{\mathcal{S}_B} c\mathbf{u} \cdot \nu \, d\sigma,$$

since $\nu_{x,t} = \nu$ on $\mathcal{S}_B \subset \partial\Omega \times (t^n, t^{n+1})$.

**The local mass constraint.** Combining, we have the *local mass constraint*

$$\int_E R\phi c^{n+1} \, dx - \int_{\hat{E}} R\phi c^n \, dx + \int_{\mathcal{S}_B} c\mathbf{u} \cdot \nu \, d\sigma = \iint_{\mathcal{E}} q_c \, dx \, dt. \tag{3.1}$$

This equation is the basis for approximation of (1.3) in the the characteristics-mixed method [2, 3], which uses piecewise discontinuous constant test functions defined over the space-time regions $\mathcal{E}$ (and the lowest order Raviart–Thomas mixed finite element [16] method for the parabolic part of the problem (1.4)).

**The local volume constraint.** A similar local mass constraint for the bulk fluid can also be derived analogously starting from the flow equation (1.1) or, equivalently, (2.1); that is, compute as above with $c \equiv 1$. Since we are dealing with incompressible fluids, we call this constraint the *local volume constraint,* and it is

$$\int_E R\phi \, dx - \int_{\hat{E}} R\phi \, dx + \int_{\mathcal{S}_B} \mathbf{u} \cdot \nu \, d\sigma = \iint_{\mathcal{E}} q \, dx \, dt. \tag{3.2}$$

As mentioned in the introduction, the reason why volume is not conserved locally is that the trace-back region $\hat{E}$ has an irregular shape, which must therefore be approximated by a simpler region $\tilde{E}$ so that the integrals in (3.1) can be evaluated. We propose to define $\tilde{E}$ as a simple octagonal shape that is approximately the original trace-back region $\hat{E}$. We do this by tracing back the four vertices and four midpoints of the edges of $E$ and then adjusting the positions of these trace-back points locally until the volume constraint is satisfied (to some acceptably small tolerance). Recall that the characteristics are the solutions of a nonlinear ordinary differential equation (2.2)–(2.3), so these are approximated numerically. Thus the trace-back points $\hat{\mathbf{x}}$ are only approximately in the correct position to begin with, so some adjustment of them to maintain a system constraint seems quite reasonable.

**4. Approximation of the integrals representing wells.** We must approximate the integral of the source function in the volume balance equation (3.2). In porous medium applications, this function models wells, which have small scales that may require special consideration.

There is no need to treat the integral representing sink (i.e., production or extraction) wells in a special way, since they simply grow in size. If $q < 0$ on element $E$, the trace-back region $\hat{E}$ contains $E$. Thus

$$\iint_{\mathcal{E}} q \, dx \, dt = \int_{t^n}^{t^{n+1}} \int_E q \, dx \, dt \quad \text{and} \quad \iint_{\mathcal{E}} q_c \, dx \, dt = \int_{t^n}^{t^{n+1}} \int_E q_c \, dx \, dt,$$

and $\hat{E}$ can be adjusted as below in section 6 to satisfy (3.2). The only caveat is that we might choose to trace more than eight points on the boundary of $E$ to obtain reasonable resolution of $\hat{E}$, since the trace-back points are diverging.

At an injection well ($q > 0$), fluid particles trace back into the well-bore where they arise. If we simply use the trapezoidal rule in time,

$$\iint_{\mathcal{E}} q\,dx\,dt \approx \frac{\Delta t}{2}\Big(\int_{\hat{E}} q^n\,dx + \int_E q^{n+1}\,dx\Big),$$

then if $\mathcal{S}_B$ is empty, the discrete volume constraint (3.2) becomes

$$\int_{\hat{E}} R\phi\,dx + \frac{\Delta t}{2}\int_{\hat{E}} q^n\,dx = \int_E R\phi\,dx - \frac{\Delta t}{2}\int_E q^{n+1}\,dx.$$

At injection, where $q > 0$, the left-hand side is positive, but the right-hand side could be *negative* if $\Delta t$ and/or $q$ is large. Thus there is no adjustment of $\hat{E}$ that will result in local volume conservation. Since we desire to use large time steps with characteristic methods, simply restricting $\Delta t$ is inappropriate.

Instead, we use a weighted trapezoidal rule with weight $w$ between 0 and 1, as in

$$\iint_{\mathcal{E}} q\,dx\,dt \approx w\Delta t\int_{\hat{E}} q^n\,dx + (1-w)\Delta t\int_E q^{n+1}\,dx, \tag{4.1}$$

so that the volume constraint becomes

$$\int_{\hat{E}} R\phi\,dx + w\Delta t\int_{\hat{E}} q^n\,dx = \int_E R\phi\,dx - (1-w)\Delta t\int_E q^{n+1}\,dx. \tag{4.2}$$

We want to define $w$ so that adjustment of $\hat{E} \subset E$ to $\tilde{E}$ results in volume conservation. We must adjust $\hat{E}$ to $\tilde{E}$ somewhere between the extreme cases of $\tilde{E} = E$ and $\tilde{E}$ being a point of size zero. That is, we need

$$\int_E R\phi\,dx + w\Delta t\int_E q^n\,dx \ge \int_E R\phi\,dx - (1-w)\Delta t\int_E q^{n+1}\,dx \ge 0, \tag{4.3}$$

so that we can define $\tilde{E}$ such that

$$\int_{\tilde{E}} R\phi\,dx + w\Delta t\int_{\tilde{E}} q^n\,dx = \int_E R\phi\,dx - (1-w)\Delta t\int_E q^{n+1}\,dx. \tag{4.4}$$

To determine an appropriate $w$, we argue as follows. Suppose that there is an injection well in element $E$. Since fluid is being injected, $q > 0$ and we expect trace-back *into* the element. Assume that $E = [-h/2, h/2]^2$ is square, $q$ and $R\phi$ are constant on $E$, the solution is symmetric near the well, and the velocity is, say, approximated by a lowest order Raviart–Thomas mixed finite element [16]. With these assumptions, the solution is found as follows. First

$$qh^2 = \int_E q\,dx\,dy = \int_E \nabla\cdot\mathbf{u}\,dx\,dy = \int_{\partial E}\mathbf{u}\cdot\nu\,d\sigma = 4\mathbf{u}\cdot\nu h,$$

since $\mathbf{u}\cdot\nu$ is assumed constant on $\partial E$. Thus $\mathbf{u}\cdot\nu = qh/4$ and the corresponding Raviart–Thomas function in $E$ is

$$\mathbf{u}(x,y) = \frac{q}{2}\begin{pmatrix} x \\ y \end{pmatrix}.$$

It is now easy to follow the characteristics (2.2)–(2.3). For $\mathbf{x} \in E$, we have that

$$\hat{\mathbf{x}}(x) = \mathbf{x}\exp\big(q(t-t^{n+1})/2R\phi\big),$$

and so $\hat{E} = [-e^{-\alpha/2}h/2, e^{-\alpha/2}h/2]^2$, where $\alpha = q\Delta t/R\phi \in (0,\infty)$. Thus the volume balance equation (3.2) is

$$R\phi h^2 - e^{-\alpha}R\phi h^2 = \int_{\mathcal{E}} q\,dx\,dt \approx [e^{-\alpha}w + (1-w)]q\Delta t\,h^2,$$

applying the weighted trapezoidal rule to the time integration. We choose the weight $w$ so that this volume balance approximation is exact; that is,

$$w = w(\alpha) = \frac{1}{1-e^{-\alpha}} - \frac{1}{\alpha}. \tag{4.5}$$

Note that $w(0^+) = 1/2$, $w(+\infty) = 1$, and

$$w'(\alpha) = \frac{-e^{-\alpha}}{(1-e^{-\alpha})^2} + \frac{1}{\alpha^2} = \frac{1}{4\sinh^2(\alpha/2)}\left[\left(\frac{\sinh(\alpha/2)}{\alpha/2}\right)^2 - 1\right] \geq 0,$$

since $\sinh(\beta) \geq \beta$ for $\beta \geq 0$. It follows that

$$1/2 \leq w(\alpha) < 1 \quad \text{for all } \alpha > 0.$$

Now in the general case we should define $w$ by (4.5) using

$$\alpha = \frac{\int_E q^{n+1}\,dx\,\Delta t}{\int_E R\phi\,dx}. \tag{4.6}$$

Since $w < 1$, we have the first inequality in (4.3), and the second follows easily. Adjustment of $\hat{E}$ in section 6 can then result in satisfaction of the volume constraint (4.2). Once this is done, the mass constraint (3.1) is then computed analogously from

$$\begin{aligned}\int_E R\phi c^{n+1}\,dx - \int_{\hat{E}} R\phi c^n\,dx + \int_{\mathcal{S}_B} c\mathbf{u}\cdot\nu\,d\sigma \\ = w\Delta t\int_{\hat{E}} q_c^n\,dx + (1-w)\Delta t\int_E q_c^{n+1}\,dx.\end{aligned} \tag{4.7}$$

We remark that the weighted trapezoidal rule is accurate to order $\Delta t$, which is the same rate of convergence in time expected of the characteristics-mixed method (see [3]). The trapezoidal rule itself is accurate to order $\Delta t^2$ but gives worse results over time because it leads to violation of local volume balance.

**5. Approximation of inflow boundaries.** Inflow boundaries are similar to internal sources in that particles trace to the boundary where they enter the system. Again, some care is needed to approximate this process. We use a technique that allows us to "trace out of the domain" in some sense. The term of concern in the volume balance equation (3.2) is

$$\int_{\mathcal{S}_B} \mathbf{u}\cdot\nu\,d\sigma,$$

which has an irregular shape on the space-time boundary $\partial\Omega\times(t^n,t^{n+1})$. The idea is to "fold" the time axis down to the $xy$-plane to create a "ghost region" (see Figure 5.1) by extending the spatial domain by an amount $t^{n+1}-t^n$ outside $\Omega$ across the inflow boundary. (The figure shows a relatively weak inflow for which no element is traced

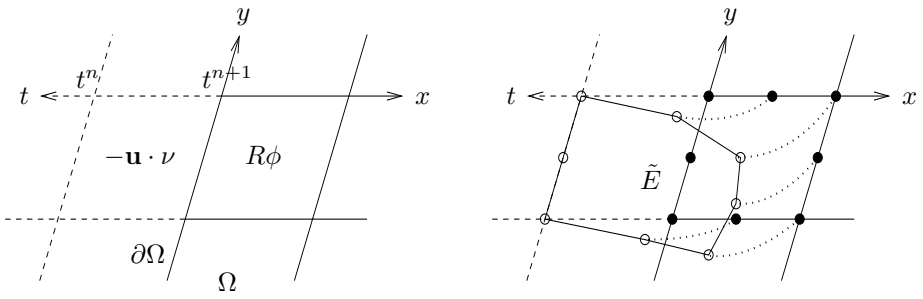


FIG. 5.1. *The inflow space-time boundary "folded" into the xy-plane, and the space-time trace-back region* $\tilde{E}$.

entirely into the folded region; however, it is possible to trace several layers of elements back into this region.)

Given an element $E$, one traces a vertex or midpoint from time $t^{n+1}$ as usual. The only question is what velocity to use outside the domain $\Omega$. One uses unit speed in the direction of $\nu$, so that the points lying on the inflow boundary of $\Omega$ trace to the $t = t^n$ boundary of the folded domain.

This procedure defines the generalized space-time trace-back region $\tilde{E}$, which is decomposed into $\tilde{E} \cap \Omega$, the usual trace-back region, and a piece $\tilde{\mathcal{S}}_B = \tilde{E} \setminus \tilde{E} \cap \Omega$ which approximates $\mathcal{S}_B$. Thus the volume constraint is simply

$$\int_E R\phi\,dx - \int_{\tilde{E}\cap\Omega} R\phi\,dx + \int_{\tilde{\mathcal{S}}_B} \mathbf{u}\cdot\nu\,d\sigma = \int_E R\phi\,dx - \int_{\tilde{E}} R\phi\,dx = \iint_{\mathcal{E}} q\,dx\,dt, \tag{5.1}$$

wherein $R\phi$ is defined to be $\mathbf{u}\cdot\nu$ in the ghost region.

The local mass constraint defining the characteristics method is similarly computed by replacing the quantity $R\phi c^n$ by $c_I^n \mathbf{u}\cdot\nu$ in the ghost region, where $c_I^n$ is the given inflow concentration; that is, we have simply

$$\int_E R\phi c^{n+1}\,dx - \int_{\tilde{E}} R\phi c^n\,dx = \iint_{\mathcal{E}} q_c\,dx\,dt. \tag{5.2}$$

In the way described in this section, we avoid explicit reference to the inflow boundary and reduce its computations to the same ones used in the interior of the domain. There is no need to treat outflow boundaries in a special way, since the trace-back region will remain within the spatial domain $\Omega$. An alternative is to use the trace-forwarding idea of section 7, especially if the flow is quite strong.

**6. Trace-back volume adjustment.** We begin the process by tracing back the four vertices $\{\mathbf{x}_{i,j},\ \mathbf{x}_{i+1,j},\ \mathbf{x}_{i,j+1},\ \mathbf{x}_{i+1,j+1}\}$ and the four midpoints of the four edges $\{\mathbf{x}_{i+1/2,j},\ \mathbf{x}_{i+1/2,j+1},\ \mathbf{x}_{i,j+1/2},\ \mathbf{x}_{i+1,j+1/2}\}$ of $E_{i,j} \in \mathcal{T}$ to form an octagon $\tilde{E}$ approximating $\hat{E}$ with corner points $\{\hat{x}_{i,j},\ \hat{x}_{i+1,j},\ \hat{x}_{i,j+1},\ \hat{x}_{i+1,j+1},\ \hat{x}_{i+1/2,j},\ \hat{x}_{i+1/2,j+1},\ \hat{x}_{i,j+1/2},\ \hat{x}_{i+1,j+1/2}\}$. We continue to call the first four corner points "vertices," and the last four "midpoints." We adjust only these eight points to enforce the local volume constraint.

We assume in this section that every element traces back without hitting the boundary of the domain. This is always possible using the space-time "folding" technique presented in section 5. That is, we may trace an element $E$ out of $\Omega$ as described,

and obtain what for algorithmic purposes looks like an octagon $\tilde{E}$ that can be adjusted as needed.

Our only restriction is related to external boundaries with no-flow, where we should respect this condition and disallow certain adjustments. If $\mathbf{x} \in \partial\Omega$ and the velocity field arises from the Stokes or Navier–Stokes equations with $\mathbf{u}(\mathbf{x}) = 0$, we should not allow any adjustment of the point $\hat{\mathbf{x}} = \mathbf{x}$. If only $\mathbf{u}(\mathbf{x}) \cdot \nu(\mathbf{x}) = 0$, we should not allow adjustment of $\hat{\mathbf{x}}$ in the normal direction (unless perhaps $\mathbf{x}$ traces back along $\partial\Omega$ to a point where the boundary condition changes to a type that allows such movement).

**6.1. Trace-back point adjustment along characteristics.** When adjusting trace-back points, care must be taken to avoid introducing systematic bias into the transport computation. We use an idea first described by Douglas, Huang, and Pereira [10], who achieved a *global* mass balance in the modified method of characteristics [12] by adjusting the trace-back points *in time.* That is, the trace-back points are adjusted in the direction of the flow field, along the characteristics, so that no bias is introduced into the *direction* of the flow. The effect is to convert spatial errors into time errors. Spatial errors tend to grow over time, but time errors are better behaved. However, Douglas, Huang, and Pereira applied their idea globally to all points simultaneously each time step. We will apply the idea locally in space.

To adjust a group of trace-back points, simultaneously adjust all of them by solving the characteristic governing equation (2.2) over a time interval $\tau^n \le t < t^{n+1}$ for some $\tau^n \approx t^n$. This changes each position along the characteristic by a small amount proportional to the local speed and the difference $\tau^n - t^n$.

We begin our trace-back point adjustment near external sources of bulk fluid, either injection wells or inflow boundaries, and proceed outward in "layers," as described subsequently.

**6.2. Trace-backs near external sources.** Using the integral approximation described in section 4, we adjust simultaneously each trace-back point of an injection well boundary until its volume is within tolerance of the target value given by (4.2). Consider now these trace-back points as being fixed in position.

For inflow boundaries, we fix the trace-back of the boundary points into the ghost region, as in section 5.

These techniques work well for milder flows. For stronger flow fields (or, equivalently, longer time steps), the trace-forwarding scheme of section 7 below is a better alternative.

**6.3. Trace-back adjustment of layers away from sources.** Once an external source has been treated, we proceed to adjust the layer of adjoining elements to obtain volume conservation in two steps, as illustrated in Figure 6.1. These adjustments are computationally quite fast.

First, simultaneously adjust all the trace-back points on the nonfixed boundary of the layer along the characteristics in time. That is, solve (2.2) over a time interval $\tau^n \le t < t^{n+1}$ for some $\tau^n \approx t^n$, so that the sum of the volumes of the elements in the layer meets the volume constraint (3.2), which in the absence of other sources, inflow boundaries, and sinks is simply

$$\sum_{E \text{ in the layer}} \int_E R\phi \, dx = \sum_{E \text{ in the layer}} \int_{\tilde{E}} R\phi \, dx.$$

We meet this constraint to some small tolerance using a type of "bisection" algorithm

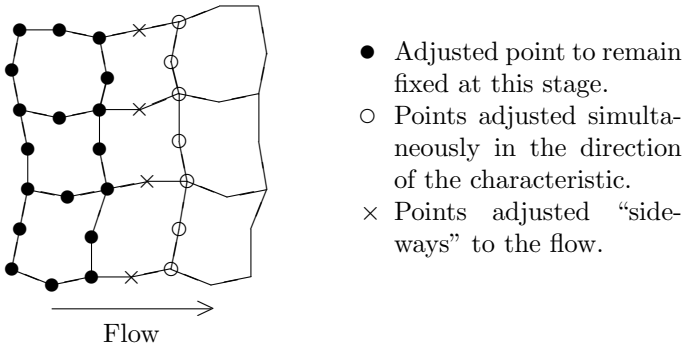


FIG. 6.1. *The adjustment of the trace-back regions. At each adjustment stage, the points marked with a solid dot remain fixed. In the first step, the points marked with a circle are simultaneously adjusted to obtain volume balance of the entire layer. In the second step, the points marked with a cross are adjusted to obtain volume balance for each element.*

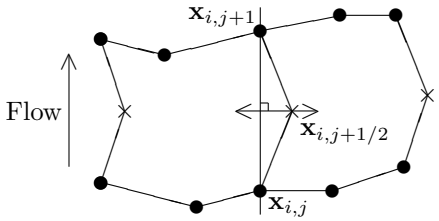


FIG. 6.2. *The adjustment of the interior midpoints. The points marked with a solid dot remain fixed, and the points marked with a cross are adjusted to obtain volume balance for each element.*

converging to the correct $\tau^n$. This method works well since points trace toward the sources backward in time, and so $\tau^n < t^n$ adjusts the region to have less volume while $\tau^n > t^n$ gives more volume. At the conclusion of this step, we have volume balance for the layer, but not for each element.

The second step is to adjust the interior midpoints of the layer to obtain volume balance of each element. We choose to adjust in the direction of maximal change to the volume (so that points move minimally). As depicted in Figure 6.2, we adjust, e.g., $\mathbf{x}_{i,j+1/2} = (x_i, y_{j+1/2})$ along the line through its unadjusted position and perpendicular to the line adjoining vertices $\mathbf{x}_{i,j}$ and $\mathbf{x}_{i,j+1}$. On an exterior no-flow boundary where $\mathbf{u}(\mathbf{x}) \cdot \nu(\mathbf{x}) = 0$, points should not be adjusted, since they can move only tangentially along the boundary, and so do not change volumes.

The trace-back layers can be of several types. Around an injection well, we may have a closed ring, in which case we may fix one of the midpoints and adjust the rest in sequence around the ring. The volume of the entire ring is correct, so adjustment of the last point will correct the volumes of the final two elements. We may also have a simple layer which meets the external boundary on two ends. Even if we are not allowed to change the end trace-back midpoints (because of no-flow boundary conditions), again we can meet the volume constraint for each element since the entire layer has the proper volume.

Things get more complex with multiple injection wells and/or inflow boundaries, since these can produce multiple basins of attraction. In that case, care must be taken when multiple trace-back adjustment layers intersect. In principle this problem can be resolved, either through human intervention or automatically. Automatic handling

involves analyzing intricate topological complexities that are beyond the scope of this work and are left for future research.

For small times, the trace-back regions of elements are well defined. However, if the time step is too large, an approximate trace-back region $\tilde{E}$ might intersect itself. This is unacceptable, and it indicates that the boundary of the true trace-back region $\hat{E}$ is convoluted (we should conclude this also if $|\tau^n - t^n|/\Delta t$ is relatively large). In this case one should either increase the number of points traced per element edge or, more practically, reduce the time step. This is in principle the only limitation on the time step $\Delta t$. This problem is most prevalent near injection wells, and we present an alternative strategy in the next section.

**7. Trace-forwarding of strong injection wells (and inflow boundaries).** Near injection wells, we have observed that before adjustment, relative volume errors of the trace-back regions $\tilde{E}$ can easily exceed 100%; thus, we must handle these regions carefully. The basic problem is that, when tracing backward in time, regions trace *into* the very small well-bore, significantly distorting the boundary of the true trace-back regions $\hat{E}$ near the well. The natural solution is to trace forward in time instead of backward. This idea was first advocated by Healy and Russell [13].

We trace points forward in time by solving the time-forward equation for the characteristics

$$\frac{d\check{\mathbf{x}}}{dt} = \frac{\mathbf{u}(\check{\mathbf{x}}, t)}{R(\check{\mathbf{x}})\phi(\check{\mathbf{x}})}, \quad t^n < t \le t^{n+1}, \tag{7.1}$$

$$\check{\mathbf{x}}(t^n) = \mathbf{x}. \tag{7.2}$$

The time-forward local volume constraint for element $E$, analogous to (3.2), is

$$\int_{\check{E}} R\phi \, dx - \int_E R\phi \, dx + \int_{\mathcal{S}_{f,B}} \mathbf{u} \cdot \nu \, d\sigma = \iint_{\mathcal{E}_f} q \, dx \, dt, \tag{7.3}$$

where now

$$\mathcal{E}_f = \{(\check{\mathbf{x}}, t) \in \Omega \times [t^n, t^{n+1}] : \check{\mathbf{x}} = \check{\mathbf{x}}(\mathbf{x}; t) \text{ for some } \mathbf{x} \in E\}$$

and $\mathcal{S}_{f,B} = \mathcal{E} \cap \partial\Omega \times [t^n, t^{n+1}]$.

We present now a technique for handling strong injection wells that replaces the ideas of section 4. It has four main steps, and is illustrated in Figure 7.1. Let $W$ represent the element containing the well (we tacitly assume the well fills the element).

First, we define the initial region $\tilde{W}$. The region of space filled by fluid from the well, $\check{W}$, is defined by tracing each point on $\partial W$ forward in time. This region is approximated by a polygon $\tilde{W}$, given by joining the traces of a finite number of boundary points. As mentioned in section 4, we might choose to trace more than our customary eight boundary points to obtain reasonable resolution of $\check{W}$, since now the trace-forward points diverge.

The second step is to adjust $\tilde{W}$ so that it satisfies the volume constraint. We simultaneously adjust the boundary points in time by solving (7.1) over the perturbed time interval $t^n < t \le \tau^{n+1} \approx t^{n+1}$ until the time-forward local volume constraint (7.3) is satisfied by the well, which is

$$\int_{\tilde{W}} R\phi \, dx = \int_W R\phi \, dx + \iint_{\mathcal{E}_f} q \, dx \, dt, \tag{7.4}$$

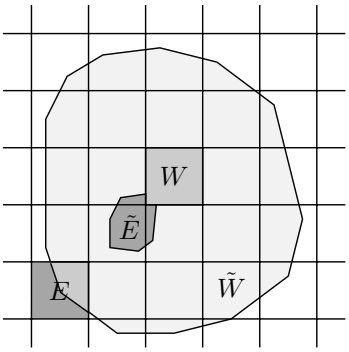


$W$ is the injection well element.
$\tilde{W}$ is the approximation to the trace-forward of $\partial W$.
$E$ is an element cut by $\partial\tilde{W}$.
$\tilde{E}$ is the approximation to the trace-back of $E \setminus \tilde{W}$.

FIG. 7.1. *Trace-forwarding around an injection well. Over the time step, part of the fluid that flows into $E$ comes from $\tilde{E}$, and the rest comes from the well $W$.*

assuming no flow on $\mathcal{S}_{f,B}$, wherein, assuming $q$ vanishes outside $W$, $\mathcal{E}_f$ can be replaced by $W \times [t^n, t^{n+1}]$.

Consider now an element $E$ affected by the well, i.e., such that $E \cap \tilde{W} \neq \emptyset$. Our third step is to define $\tilde{E}$. Points within $\tilde{W}$ need not be traced back, since we know that they trace into the well. Thus, if $E \subset \tilde{W}$, $\tilde{E} = \emptyset$. So consider an $E$ cut by $\partial\tilde{W}$ (i.e., $E \cap \partial\tilde{W} \neq \emptyset$). We trace back any of our usual eight points on $\partial E$ that lie outside $\tilde{W}$. We also trace back the (most likely two) points $\partial E \cap \partial\tilde{W}$, which must trace to $\partial W$ (if not, simply adjust the time interval so as to hit the well). Polygonal approximation defines a region $\tilde{E}$ outside $W$.

The fourth and final step is to adjust $\tilde{E}$ to satisfy the local volume constraint. We simultaneously adjust the points of $\partial\tilde{E}$ not on $\partial W$ backward in time using (2.2) over a time interval $t^n \approx \tau^n \leq t < t^{n+1}$ to satisfy the local volume constraint outside the well, which is

$$\int_E R\phi \, dx = \int_{\tilde{E}} R\phi \, dx + \frac{|E \cap \tilde{W}|}{|\tilde{W}|} \iint_{W \times [t^n, t^{n+1}]} q \, dx \, dt,$$

since the region $E \cap \tilde{W}$ receives a proportional amount of fluid from the well.

We note that the transport itself, given above in the local mass constraint (3.1), is correspondingly modified as

$$\int_E R\phi c^{n+1} \, dx = \int_{\tilde{E}} R\phi c^n \, dx + \iint_{W \times [t^n, t^{n+1}]} q_c \, dx \, dt.$$

A similar construction can be applied near strong inflow boundaries. In that case, the construction of section 5 is not needed, since points no longer trace out of the domain.

**8. Numerical experiments.** In this section we illustrate the volume balance techniques in five examples. The last example has an analytic solution, but in the others, we determine the Darcy velocity $\mathbf{u}$ of the fluid in terms of the pressure $p$ according to Darcy's law:

$$\mathbf{u} = -\frac{k}{\mu} \nabla p, \tag{8.1}$$

where $\mu$ is the viscosity and $k$ is the permeability. We assume that the wells $q$ are independent of time $t$, so that it suffices to solve for $\mathbf{u}$ once from the divergence constraint (1.1), subject to the boundary conditions, which vary with the example.

We assume that $\mu$ is constant (i.e., the concentrations of the components are too small to affect the viscosity of the fluid), and has the value 0.01 poise (i.e., water) in our examples. However, $k$ varies with the example, and it is heterogeneous. A measure of the variability of $k$ is given by the dimensionless coefficient of variation

$$C_v = \frac{1}{\mu_k}\left(\frac{1}{|\Omega|}\int_\Omega (k(x)-\mu_k)^2\,dx\right)^{1/2}, \tag{8.2}$$

which is the ratio of the standard deviation of $k$ and its mean value

$$\mu_k = \frac{1}{|\Omega|}\int_\Omega k(x)\,dx. \tag{8.3}$$

Since the local volume constraint is really local conservation of the bulk fluid, we believe that it is important to use a locally conservative method to approximate the solution of (8.1). We use a standard lowest order Raviart–Thomas mixed method [16] implemented as cell-centered finite differences [17, 4].

We will be solving (1.2), wherein the diffusion/dispersion tensor $D$ is given by the formula

$$D = \phi\, d_{\mathrm{mol}} I + |\mathbf{u}|[(d_{\mathrm{long}} E(\mathbf{u}) + d_{\mathrm{trans}} E^{\perp}(\mathbf{u}))], \tag{8.4}$$

where $E(\mathbf{u})$ denotes projection along the vector $\mathbf{u}$, $E^{\perp}(\mathbf{u})$ its orthogonal complement, and where the molecular diffusion coefficient $d_{\mathrm{mol}} = 10^{-7}$ cm$^2$/sec, the longitudinal dispersion coefficient $d_{\mathrm{long}} = 10^{-3}$ cm, and the transverse dispersion coefficient $d_{\mathrm{trans}} = 10^{-4}$ cm. Again we use Raviart–Thomas spaces to approximate this part of the operator (see [2, 3] for details).

In this section, we contrast our three schemes: the unmodified characteristics-mixed method (CMM) [2, 3], our volume conserving CMM without trace-forwarding of the well (VCCMM), and our volume conserving CMM with trace-forwarding of the well (VCCMM-TF).

**8.1. A nuclear contamination problem.** In our first example, we describe a nuclear contamination problem in a water saturated porous medium. The domain $\Omega$ is a square of size 256 m $\times$ 256 m. The permeability $k$ is depicted in Figure 8.1. The

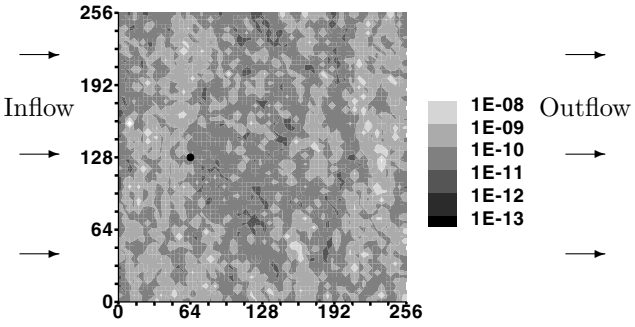


FIG. 8.1. *The nuclear contamination problem domain and permeability field, in cm$^2$. The location of the injection well is marked with a black dot at* $(64, 128)$.

permeability is log-normal and fractal, with mean $2 \times 10^{-10}$ cm$^2$ (about 20 md) and a variation of over five orders of magnitude from around $10^{-13}$ to $10^{-8}$ cm$^2$ (about 0.01 md to 1 darcy). Its coefficient of variation (8.2) is $C_v = 0.522$.

Our assumption that $\mu$ is constant merely says that the concentrations of the nuclear components are too small to affect the viscosity of the fluid. We impose the boundary conditions of no normal flow $\mathbf{u}\cdot\nu = 0$ on the "top" and "bottom" faces of the domain ($y = 0$ m and $y = 256$ m, respectively), and a constant pressure at the left face of $5 \times 10^5$ g/cm·sec$^2$ and a constant pressure at the right face of $-5 \times 10^5$ g/cm·sec$^2$, giving rise to a background flow from left to right. There is a single injection well covering 4 grid cells and placed at $(64, 128)$ m. We inject one pore volume every 50 years.

We transport a decaying nuclear component of concentration $c$. It satisfies the advection-diffusion equation (1.2), with a reaction term added in:

$$(R\phi c)_t + \nabla \cdot (c\mathbf{u} - D\nabla c) = -\lambda\phi R c + q_c(c), \quad \Omega \times J. \tag{8.5}$$

We take the porosity $\phi = 0.01$, the retardation factor $R = 12$, and the decay constant (for $^{234}$U) $\lambda = 9 \times 10^{-14}$/sec. We inject into an initially clean aquifer a concentration $c_I$ of $1 \times 10^{-5}$ g/cm$^2$.

In the first set of runs, we consider a $64 \times 64$ rectangular grid and contrast four schemes: the unmodified characteristics-mixed method (CMM) [2, 3], a higher order Godunov method [18, 5, 9, 15, 1], and our volume conserving CMM with and without trace-forwarding near the well (VCCMM and VCCMM-TF).

Explicit methods in one dimension have a time step restriction [15], known as the CFL time-step, given by

$$\Delta t \le \Delta t_{\text{CFL,1-D}} = \max_{\mathbf{x}\in\Omega} \frac{hR\phi(x)}{|\mathbf{u}(\mathbf{x})|},$$

where $h$ is the grid spacing. Since we are working in two dimensions, we should limit $\Delta t$ to half this value,

$$\Delta t \le \Delta t_{\text{CFL,2-D}} = \max_{\mathbf{x}\in\Omega} \frac{hR\phi(x)}{2|\mathbf{u}(\mathbf{x})|},$$

for the Godunov method. For our $64 \times 64$ grid, the two-dimensional CFL limited time-step is 0.586 year, but we use a much larger time step for the VCCMM.

We obtain the trace-back regions by tracing back the corners and midpoints of each grid element, and connecting the points by straight lines. On the left side of Figure 8.2, we plot these trace-back regions near the injection well for the CMM and the corresponding volume (i.e., area) errors, using a time step of only 1.5 years, which is about 3 times the CFL limit. We see up to 292% volume balance error at the well. Most of the regions are beyond $\pm 1\%$, and many beyond $\pm 10\%$. Starting from these trace-back regions, the VCCMM adjustment algorithm (without trace-forwarding around the well) gives the trace-back regions on the right side of Figure 8.2, in which only floating point rounding error is observed (up to only about $10^{-9}$ volume balance error).

We show the contour plots of the contaminant concentration $c$ at 30 years in Figures 8.3 and 8.4 for the four methods. The shape and sharpness of the front, and the presence of undershoot or overshoot, are to be noted. The CMM, while locally mass conservative, does not conserve volume, so the concentrations exhibit

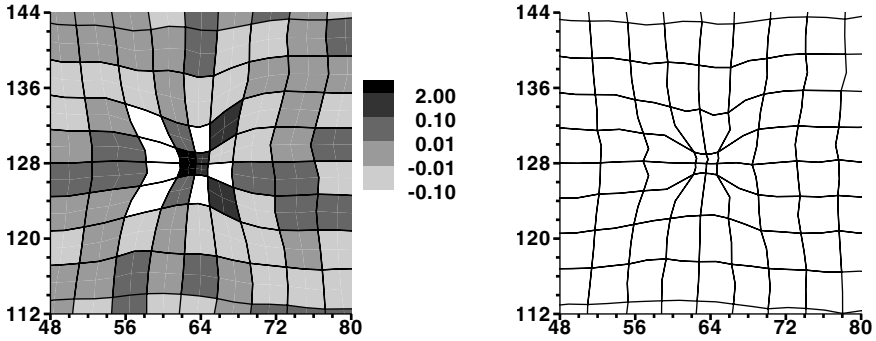


FIG. 8.2. *The nuclear contamination problem trace-back regions near the well, with CMM on the left and VCCMM (without trace-forwarding near the well) on the right. The relative volume errors are shown for CMM. The VCCMM volume errors are on the order of* $10^{-9}$.

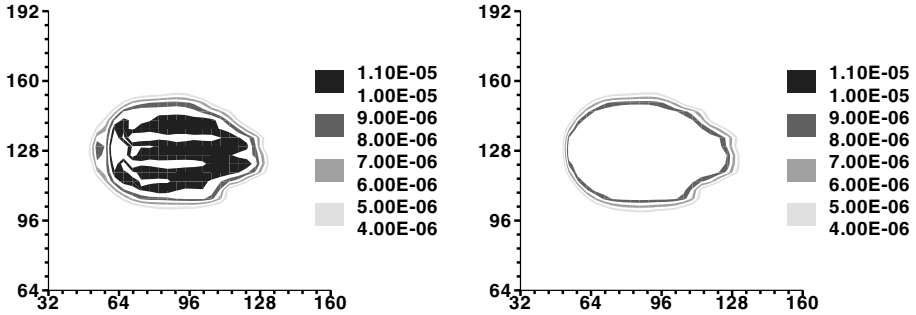


FIG. 8.3. *The nuclear contamination problem CMM (left) and VCCMM (right) concentration at* 30 *years on the* $64 \times 64$ *grid, in g/cm*$^2$*, using a time step of* 1.5 *years.*

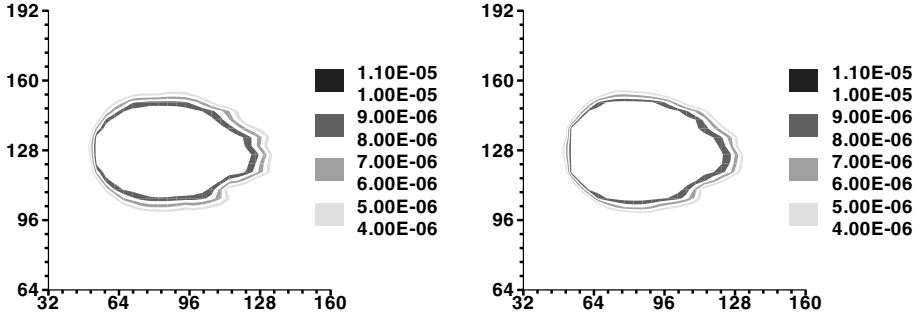


FIG. 8.4. *The nuclear contamination problem higher order Godunov (left) and VCCMM-TF (right) concentration at* 30 *years on the* $64 \times 64$ *grid, in g/cm*$^2$*. We used the CFL time step* 0.586 *year for Godunov and* 3 *years for VCCMM-TF.*

significant overshoot, reaching 134% of the maximum possible value near the well using a time step of 1.5 years. Moreover, volume nonconservation introduces many nonphysical local minima and maxima into the solution. The VCCMM corrects these problems and gives a solution very similar to the higher order Godunov method using $\Delta t = 0.586$ year. Moreover, attention to the well in the VCCMM-TF allows us to use a much larger time step of 6 years. These three methods exhibit no undershoot

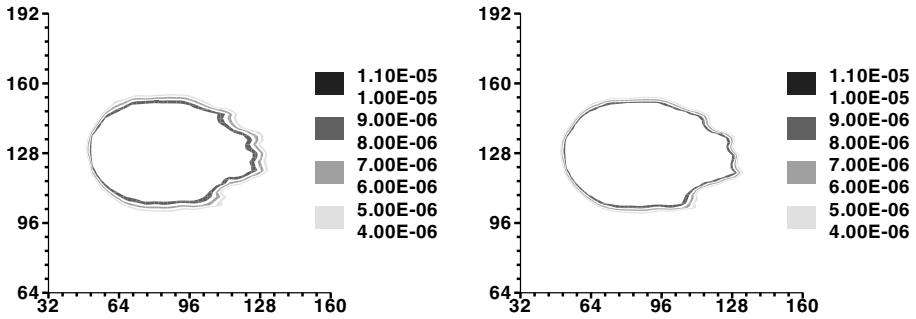


FIG. 8.5. *The nuclear contamination problem higher order Godunov (left) and VCCMM-TF (right) concentration at* 30 *years on the* $128 \times 128$ *grid, in g/cm*$^2$. *We used the CFL time step* 0.146 *years for Godunov and* 1 *year for VCCMM-TF.*

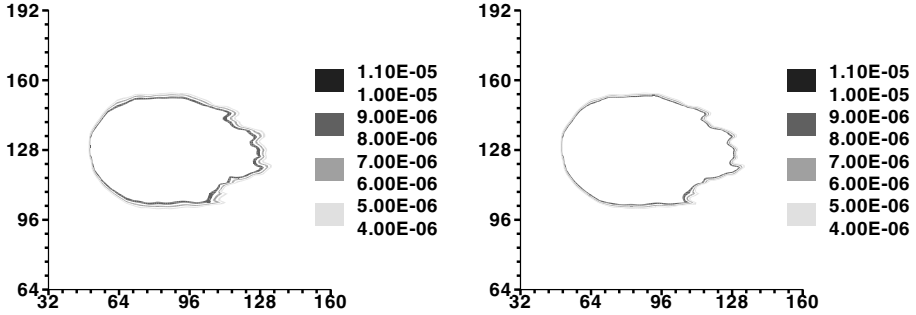


FIG. 8.6. *The nuclear contamination problem higher order Godunov (left) and VCCMM-TF (right) concentration at* 30 *years on the* $256 \times 256$ *grid, in g/cm*$^2$. *We used the CFL time step* 0.0366 *years for Godunov and* 0.5 *years for VCCMM-TF.*

or overshoot, and each predicts a similar front shape. However, the VCCMM and VCCMM-TF are less numerically diffuse, in that the front is sharper (due primarily to using a larger time step).

Finally, in Figures 8.5 and 8.6, we show the results of using finer grids: $128 \times 128$ and $256 \times 256$. The front sharpens under refinement, indicating that most of the spread is indeed due to the numerical methods and not the physical diffusion and dispersion. Again, the higher order Godunov and VCCMM-TF give comparable results, but the VCCMM-TF is somewhat less numerically diffusive and uses a much larger time step. The CFL step for the $128 \times 128$ grid is $\Delta t_{\text{CFL,2-D}} = 0.146$ years (205 steps to 30 years), but the VCCMM-TF used $\Delta t = 1$ year (30 steps), which is 6.8 times the CFL limit. For the $256 \times 256$ grid, $\Delta t_{\text{CFL,2-D}} = 0.0366$ years (820 steps), but the VCCMM-TF used $\Delta t = 0.5$ years (60 steps), which is 13.7 times the CFL limit.

**8.2. A quarter five-spot flood.** The second example is related to miscible flooding in a petroleum reservoir. We consider a quarter of a "five-spot" pattern of wells, which is a rectangular domain with an injection well in the lower left corner and a production well in the upper right corner, and no-flow (homogeneous Neumann) boundary conditions. Our domain is $40 \times 40$ meters square, and we impose an $80 \times 80$ grid over the domain. It is initially clean: $c(\mathbf{x}, 0) = 0$. The injector covers 4 cells near the corner $(0, 0)$ meters and has a rate of 1 pore volume every 5 years, injecting an inert tracer with concentration $c_I = 1$. The 4 cell comprising the producer are near the

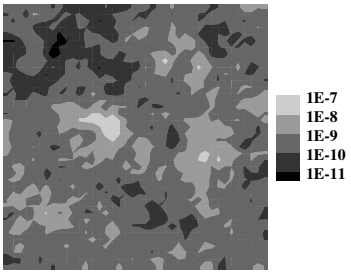


FIG. 8.7. *The quarter five-spot permeability field, in* $cm^2$.

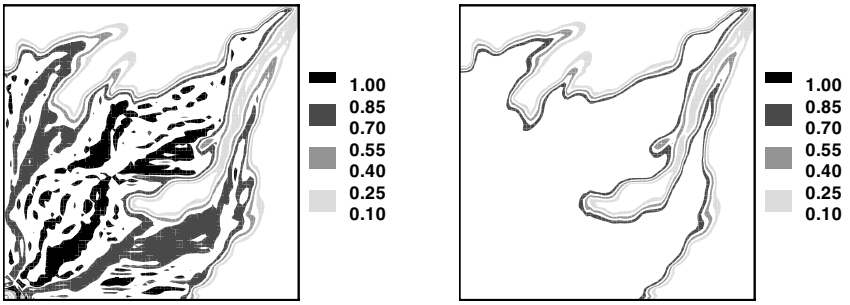


FIG. 8.8. *The quarter five-spot CMM (left) and VCCMM (right) concentration at* 3.36 *years.*

opposite corner $(40, 40)$ meters and its rate is opposite that of the injector. We solve (1.2) with no retardation (i.e., $R = 1$), no reactions, a constant porosity of 0.25, and the heterogeneous permeability $k$ depicted in Figure 8.7, which was geostatistically generated and has mean 100 md ($10^{-9}$ cm$^2$) and $C_v = 2.58$ and varies by about 4 orders of magnitude.

In Figure 8.8 we plot the results at 3.36 years using 280 steps of 0.012 year/step, which is 10.68 times the 2-D CFL number. The CMM shows both overshoot and undershoot in what should be the swept region, while the VCCMM shows no such artifacts. The poor performance of the CMM can be attributed to the extreme local heterogeneity of the permeability ($C_v = 2.58$), which produces large volume imbalances throughout the domain. In fact the field is so heterogeneous that a slightly larger time step of 0.0136 year/step (12.10 times the CFL number) initially creates degenerate trace-back regions, which cannot be used.

**8.3. A fluvial domain.** The third example is related to a fluvial geological environment that is correlated over large distances. The problem is taken from White and Horne [19], and the permeability is depicted in Figure 8.9, which clearly shows an ancient river bed with high permeability. We use only three values for the permeability, with mean 4.056 Darcy and $C_v = 1.15$. The domain is $600 \times 600$ feet squared and posed on a $30 \times 30$ grid. There is an injection well at grid cell $(1, 1)$ and a production well at grid cell $(30, 30)$. The injection concentration is $c_I = 1$, and the rate is 1 pore volume every 3 years. The production rate is opposite, and there are no-flow boundary conditions. The porosity is constant at 0.2, and $c$ is initially set to zero. We solve the problem on a refined $60 \times 60$ computational grid to improve resolution (with wells now filling 4 cells). We use a time step of 0.015 years, which is 12.84 times the 2-D CFL limit.

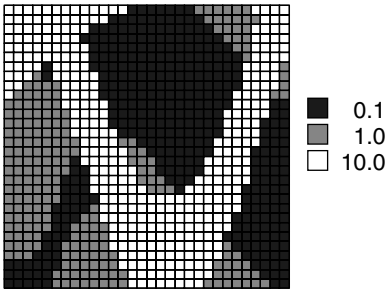


FIG. 8.9. *The fluvial domain example. The permeability field, in darcies, with the injector in the lower left and the producer in the upper right.*

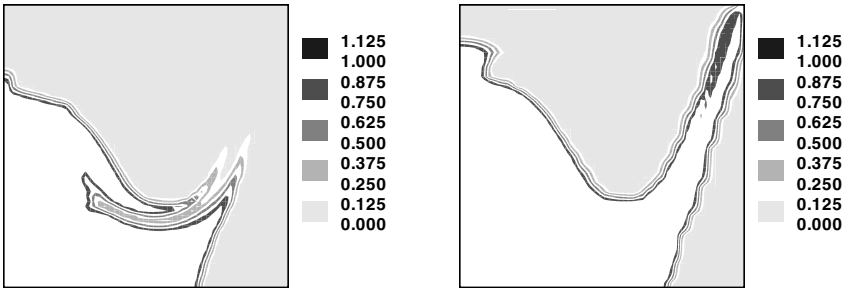


FIG. 8.10. *The fluvial domain VCCMM-TF concentration at* 1.05 *years (left) and* 1.65 *years (right).*

In Figure 8.10, we show results at 1.05 and 1.65 years (70th and 110th steps). Notice how the tracer follows the ancient river channel and avoids the lower permeability regions. The plume advances initially in time on both sides of the very low permeability region containing the well, as seen at 1.05 years, and reconnects further along in time within the very high permeability channel. As is evident at 1.65 years, within the high permeability channel, the top portion of the plume travels a greater distance, and so is retarded in position compared to the bottom half of the plume. Each half of the plume near the production well at 1.65 years is only a few grid elements in width. The plume is connected; however, the plotting routine cannot handle such a thin plume and shows some disconnection. We see a similar illusion at 1.05 years where the plume is very thin.

Serious relative volume errors are observed both at the wells and along the ancient riverbank, where a "stair-step" pattern of grid elements is used to approximate its shape. Using initial trace-back regions, the wells are so poorly approximated that the CMM actually produces negative concentrations on a $30 \times 30$ grid and time step of only 0.01 years, indicating a twisting of the trace-back regions so that they self intersect.

To isolate the riverbank errors, we applied only the trace-forwarding well adjustment to the injection well and adjusted volumes near the production well. The result of CMM using this partially processed trace-back mesh is depicted in Figure 8.11. We obtained significant improvement over straight CMM (not pictured), but the front is advanced in the CMM results compared to the VCCMM-TF, since the CMM with well adjustment simulation has average concentrations in the plume below 0.875. Thus the

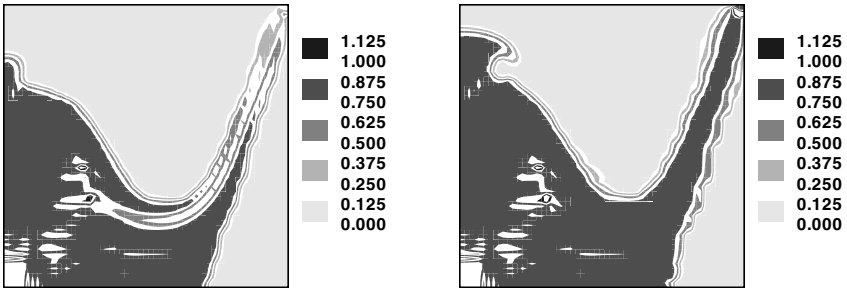


FIG. 8.11. *The fluvial domain CMM with well adjustments only. Concentration at* 1.05 *years (left) and* 1.65 *years (right).*

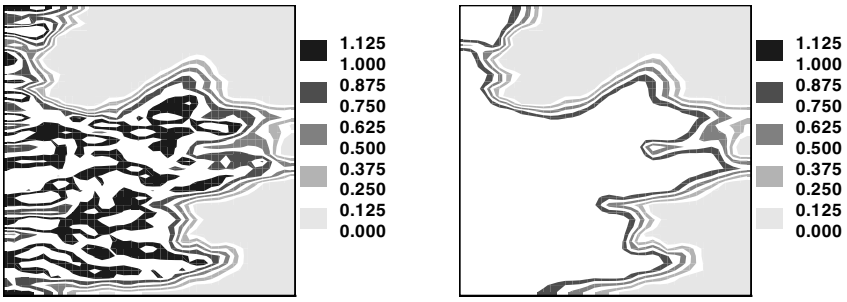


FIG. 8.12. *The linear flood CMM (left) and VCCMM (right) concentration at* 25 *years using time step* 0.18 *years. (The CFL time step is* 0.06 *years.)*

problem is not simply associated with the treatment of wells but also with treatment of trace-back regions throughout the domain. We note that the relative errors along the "stair-step" river bank reduce under grid refinement (as long as the refinement attempts to follow the true, smooth river bank).

**8.4. A linear flood.** Our fourth example tests the inflow boundary adjustment. We use the permeability field in the second example (see Figure 8.7). However, this time we assume no wells and instead impose a linear pressure drop across the domain in the $x$-direction (the pressure difference is about a tenth of that in the first example).

The time step is 0.18 years, which is three times the CFL time step. In Figure 8.12, we show results after 140 steps, or about 25 years. The CMM is very disappointing. It exhibits severe overshoots up to a concentration of 1.65 and volume errors exceed 10% in the interior of the domain. However, the VCCMM algorithm (using the ideas in section 5 to approximate the inflow boundary) was able to remove these severe volume errors, and we observe good results with mass and volume being strictly conserved.

In Figure 8.13 we show the corresponding results for the VCCMM-TF (using section 7 to treat the inflow boundary) for time steps 0.18 and 0.36 years (3 and 6 times the CFL step). As can be seen, the inflow is better approximated using VCCMM-TF. We might expect a thinner diffusion layer for the simulation using the larger time step, but evidently the grid is not fine enough to resolve this. We note that for this example, a time step 9 times CFL causes excessive initial relative volume errors inside the domain of around 25%.

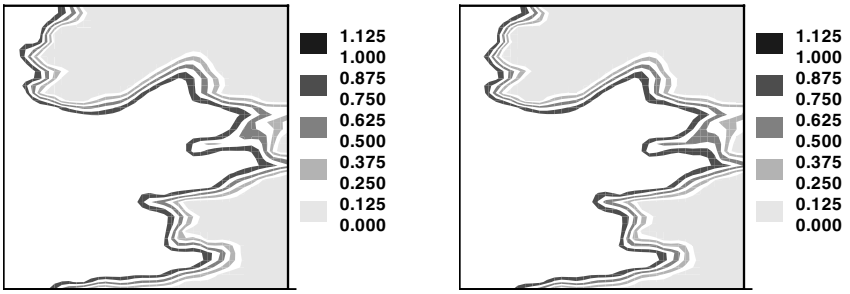


FIG. 8.13. *The linear flood VCCMM-TF concentration at* 25 *years for time steps* 0.18 *years (left) and* 0.36 *years (right). (The CFL time step is* 0.06 *years.)*

**8.5. A comparison with an analytic solution.** Our fifth and final example is to compare the VCCMM-TF to the results of an analytic solution due to Hsieh [14] involving radial flow out of a well in a horizontally infinite, uniform porous medium (effectively making the problem one dimensional). In radial coordinates, where $r$ is the radial distance from the center line of the recharge well, we have

$$\begin{aligned} &c_t + \frac{A}{r}c_r = d_{\text{long}}\frac{A}{r}c_r r, && r > r_w,\ t > 0,\\ &c(r_w,t) = c_I \quad \text{and} \quad c(+\infty,t) = 0, && t > 0,\\ &c(r,0) = 0, && r > r_w, \end{aligned}$$

where $A = Q/(2\pi b\phi)$, $Q$ is the volumetric rate of tracer injection, $b$ is the vertical thickness of the formation, $\phi$ is the porosity, $d_{\text{long}}$ is the longitudinal dispersivity, $r_w$ is the radius of the injection well, and $c_I$ is the concentration of the injected tracer. In dimensionless form, the equation is

$$G_\tau + \frac{1}{\rho}G_\rho = \frac{1}{\rho}G_{\rho\rho}, \quad \rho > \rho_w,\ \tau > 0,$$

where $G = c/c_I$, $\rho = r/d_{\text{long}}$, $\rho_w = r_w/d_{\text{long}}$, and $\tau = At/d_{\text{long}}^2$. Hsieh gave the analytic solution to this problem.

We mimic the same setting in a 2-D finite domain with the well in the center. The domain is 256 meters square and has a thickness of $b = 1$ m, porosity $\phi = 0.2$, and initial concentration $c = 0$. Fluid with a concentration $c_I = 1$ is injected into the center of the domain at the rate of $Q = 4369.06$ cubic meters per year (which is 1 pore-volume every 3 years). We also set $R = 1$ (i.e., no retardation).

We present two test cases, with either more or less dispersion. For the dispersion tensor (8.4), the less dispersive case has molecular diffusion $d_{\text{mol}} = 0.002$ cm$^2$/sec and longitudinal dispersion $d_{\text{long}} = 20$ cm. The more dispersive case is five times stronger: $d_{\text{mol}} = 0.01$ cm$^2$/sec and $d_{\text{long}} = 100$ cm.

In Figure 8.14 we show the comparison in the concentration along the radial direction away from the well. The analytic solution is derived from Hsieh's code [14]. We solve the full 2-D problem using our VCCMM-TF algorithm on a $128 \times 128$ grid and a time step of $\Delta t = 0.005$ years, which is 6.82 times the 2-D CFL limit, and report the concentration on the positive $x$-axis away from the well. On the left is the less diffusive case at time 0.2 years, and on the right is the more diffusive case at 0.1 years. As can be seen, the match is excellent.

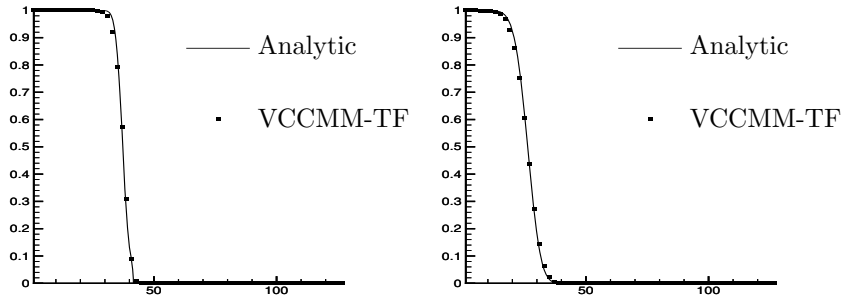


FIG. 8.14. *Comparison between the analytic and the VCCMM-TF concentration along the radial direction away from the well. On the left is the less diffusive case at time* 0.2 *years, and on the right is the more diffusive case at* 0.1 *years.*

**9. Conclusions.** A critical aspect of approximating hyperbolic transport problems is to conserve the mass of the tracer locally. As we saw in the numerical examples, it is just as critical to the conserve locally the mass of the bulk fluid. We have termed this constraint *volume conservation.* Incorrect densities, and therefore incorrect reaction dynamics, result from violation of the volume constraint. It can also lead to severe overshoot or undershoot, especially around injection wells, and even to incorrectly predicting the advancement of fronts.

We should remark that one can recover smooth densities by modifying the definition of the trace-back concentration. Simply multiply the concentration obtained for element $E$ by the correction factor $|\tilde{E}|/|E|$. This results in volume conservation, and to the eye, all the plumes appear smooth (i.e., show no overshoot or undershoot) like the VCCMM results. However, this modification destroys mass conservation.

When adjusting trace-back points, care must be used to avoid introducing systematic bias into the transport computation. We presented algorithms that produce good trace-back regions. The key is to adjust the trace-back points "in time," i.e., along the characteristics, where possible. Weaker wells and inflow boundaries can be treated with simple techniques (wells by quadrature and inflow transparently through a space-time "fold-down" strategy). For stronger wells and inflow boundaries, one should use a trace-forwarding strategy.

We do not suggest that ours is the only reasonable adjustment strategy; it is merely one of many that could be implemented. The point of the paper has been to point out how critical this step is, and to present one practical solution to the problem. We saw that our algorithms produce accurate results when compared to Godunov's method and an analytical solution. Our method also allows us to take large time steps such as 3 to 14 times the two-dimensional CFL limited time step, which results in less numerical dispersion than do explicit differencing methods such as Godunov's method.

Trace-back adjustment requires a fair amount of computation. Thus characteristic methods such as ELLAM and CMM are perhaps best suited to steady or near steady flows and long time periods or perhaps when numerical diffusion simply cannot be tolerated. These situations arise, for example, in the modeling of geologic basin formation, long-lived radio-isotope decay, or miscible fingering.

## REFERENCES

[1] T. ARBOGAST, *User's Guide to Parssim*1: *The Parallel Subsurface Simulator, Single Phase*, Tech. Rep. TICAM Report 98–13, The Center for Subsurface Modeling, Texas Institute for Computational and Applied Mathematics, The University of Texas at Austin, Austin, TX, May 1998.

[2] T. Arbogast, A. Chilakapati, and M. F. Wheeler, *A characteristic-mixed method for contaminant transport and miscible displacement*, in Computational Methods in Water Resources IX, Vol. 1: Numerical Methods in Water Resources, T. F. Russell et al., eds., Computational Mechanics Publications, Southampton, UK, 1992, pp. 77–84.

[3] T. Arbogast and M. F. Wheeler, *A characteristics-mixed finite element method for advection dominated transport problems*, SIAM J. Numer. Anal., 32 (1995), pp. 404–424.

[4] T. Arbogast, M. F. Wheeler, and I. Yotov, *Mixed finite elements for elliptic problems with tensor coefficients as cell-centered finite differences*, SIAM J. Numer. Anal., 34 (1997), pp. 828–852.

[5] J. B. Bell, C. N. Dawson, and G. R. Shubin, *An unsplit higher-order godunov scheme for scalar conservation laws in two dimensions*, J. Comput. Phys., 74 (1988), pp. 1–24.

[6] M. A. Celia, T. F. Russell, I. Herrera, and R. E. Ewing, *An Eulerian-Lagrangian localized adjoint method for the advection-diffusion equation*, Advances in Water Resources, 13 (1990), pp. 187–206.

[7] A. Chilakapati, *Numerical Simulation of Reactive Flow and Transport through the Subsurface*, Ph.D. thesis, Rice University, Houston, Texas, 1993.

[8] A. Chilakapati, *A characteristic-conservative model for Darcian advection*, Advances in Water Resources, 22 (1999), pp. 597–609.

[9] C. Dawson, *Godunov-mixed methods for advection-diffusion equations in multidimensions*, SIAM J. Numer. Anal., 30 (1993), pp. 1315–1332.

[10] J. Douglas, Jr., C.-S. Huang, and F. Pereira, *The modified method of characteristics with adjusted advection*, Numer. Math., 83 (1999), pp. 353–369.

[11] J. Douglas, Jr., F. Pereira, and L.-M. Yeh, *A locally conservative Eulerian-Lagrangian numerical method and its application to nonlinear transport in porous media*, Comput. Geosci., 4 (2000), pp. 1–40.

[12] J. Douglas, Jr., and T. F. Russell, *Numerical methods for convection-dominated diffusion problems based on combining the method of characteristics with finite element or finite difference procedures*, SIAM J. Numer. Anal., 19 (1982), pp. 871–885.

[13] R. W. Healy and T. F. Russell, *Treatment of internal sources in the finite-volume ELLAM*, in Computational Methods in Water Resources XIII, Vol. 2, L. R. Bentley, J. F. Sykes, C. A. Brebbia, W. G. Gray, and G. F. Pinder, eds., A. A. Balkema, Rotterdam, 2000, pp. 619–622.

[14] P. A. Hsieh, *A new formula for the analytical solution of the radial dispersion problem*, Water Res. Res., 22 (1986), pp. 1597–1605.

[15] R. J. LeVeque, *Numerical Methods for Conservation Laws*, 2nd ed., Birkhäuser, Basel, 1992.

[16] R. A. Raviart and J. M. Thomas, *A mixed finite element method for 2nd order elliptic problems*, in Mathematical Aspects of Finite Element Methods, I. Galligani and E. Magenes, eds., Lecture Notes in Math. 606, Springer-Verlag, New York, 1977, pp. 292–315.

[17] T. F. Russell and M. F. Wheeler, *Finite element and finite difference methods for continuous flows in porous media*, in The Mathematics of Reservoir Simulation, R. E. Ewing, ed., 1 Frontiers Appl. Math., SIAM, Philadelphia, 1983, pp. 35–106.

[18] B. van Leer, *Towards the ultimate conservative difference scheme via second-order sequel to godonov's methods*, J. Comput. Phys., 32 (1979), pp. 101–136.

[19] C. D. White and R. N. Horne, *Computing absolute transmissibility in the presence of fine-scale heterogeneity, Paper SPE* 16011, in Proceedings, Ninth SPE Symposium on Reservoir Simulation, 1987, pp. 209–220.